Yrast and non-yrast spectroscopy of ^{199}Tl using α-induced reactions

Soumik Bhattacharya,[1,2] S. Bhattacharyya,[1,2,*] R. Banik,[1,2] S. Das Gupta,[3] G. Mukherjee,[1,2] A. Dhal,[1] S. S. Alam,[1,2]
Md. A. Asgar,[1,2,†] T. Roy,[1,2] A. Saha,[1,2] S. Nandi,[1,2] T. Bhattacharjee,[1,2] A. Choudhury,[1] Debasish Mondal,[1,2]
S. Mukhopadhyay,[1] P. Mukhopadhyay,[1] S. Pal,[1] Deepak Pandit,[1] I. Shaik,[1] and S. R. Banerjee[1]

[1]*Variable Energy Cyclotron Centre, 1/AF Bidhannagar, Kolkata 700064, India*
[2]*Homi Bhabha National Institute, Training School Complex, Anushaktinagar, Mumbai-400094, India*
[3]*Victoria Institution (College), Kolkata 700009, India*

The excited states of the ^{199}Tl nucleus have been studied by using the light ion induced fusion evaporation reaction ^{197}Au$(\alpha, 2n)^{199}$Tl at 30 MeV of beam energy by γ-ray spectroscopic methods. VECC Array for NUclear Spectroscopy (VENUS) has been used to detect the prompt γ rays. Level scheme of ^{199}Tl has been significantly improved and extended with the placement of 53 new transitions. The yrast $\pi h_{9/2}$ band has been extended in this nucleus beyond the band crossing. Several new near- and non-yrast band structures have also been identified. It has been observed that in case of the three-quasiparticle structures, a different configuration involving negative parity neutron orbitals becomes yrast for heavier Tl isotopes with $N \geqslant 118$ in contrast to the involvement of the neutron $i_{13/2}$ orbital for lighter Tl isotopes. It was possible to identify both the yrast and the non-yrast states corresponding to these configurations in the present work. The observed band structures have been interpreted in light of the systematics of the neighboring odd mass Thallium nuclei. Total Routhian surface calculations have been performed to study the deformation and shape changes as a function of rotational frequency in this nucleus.

I. INTRODUCTION

Thallium isotopes, with only one proton below the $Z = 82$ shell closure, are the most appropriate candidates to extend our knowledge on the polarizing effect of the high-j proton intruder orbitals (e.g., $\pi h_{9/2}$, $\pi i_{13/2}$) or high-j neutron orbitals (e.g., $\nu i_{13/2}$) on the shape of a nucleus, which are otherwise near-spherical at their ground state. Several interesting and exotic phenomena, like magnetic rotational bands [1] and chiral bands [2–4] have been reported in the thallium isotopes around the $A \sim 200$ mass region. It is, therefore, interesting to investigate the interplay of the single particle structures (involving high-j orbitals) and the collectiveness of the underlying core that generates the above exotic phenomena, below the $Z = 82$ shell closure region [5–7]. It is known that the high-j orbitals, specially, $\pi h_{9/2}$ and $\nu i_{13/2}$, induce oblate shape in the nuclei in this region [8]. In the case of the odd-A Tl nuclei, a wide diversity of shapes and structures have been observed from superdeformed structures in neutron deficient ^{191,193,195}Tl [9–11] to weakly deformed oblate band structures in ^{191,193,195,197,201}Tl [12–15], depending on the neutron Fermi level and the excitation energy. In the heavier isotope ^{205}Tl, which is close to the doubly magic ^{208}Pb nucleus, excited states corresponding to the octupole core excitation was also observed [16]. Although deformed shapes based on the $\pi i_{13/2}$ intruder orbital have been observed for the lighter Tl isotopes,

no such band structure has been reported in heavier odd-mass thallium isotopes. A survey of the excitation energies of these states in the heavier isotopes indicates that it becomes more and more non-yrast with the increase in neutron number [17]. In the neighboring isotope ^{197}Tl, an excited state corresponding to the $\pi i_{13/2}$ orbital has been reported but no band structure was observed on top of this state [18].

It is interesting to note that the shape polarizing effect of the $\pi h_{9/2}$ orbital continues to generate deformed band structures for the isotopes ^{200,201}Tl, as reported in our previous work [15,19]. However, the three-quasiparticle configuration, observed after the band crossing of the $\pi h_{9/2}$ oblate band, in the $N = 120$ isotope ^{201}Tl was observed to be different with smaller gain in aligned angular momentum compared to the other lighter isotopes. This is possibly because of the fact that the neutron Fermi level moves up and away from the $\nu i_{13/2}$ orbital with the increase in neutron number. For spherical shape, the neutron Fermi level is expected to be situated around the $3p_{3/2}$ orbital above the $i_{13/2}$ orbital for $N \geqslant 114$. However, for oblate deformation, as it is the case for the Tl isotopes, it would move up to lie close to the $2f_{5/2}$ orbital for $N \geqslant 118$. Therefore, it is important to study the band crossing behavior of ^{199}Tl to understand the relative position of the $\nu i_{13/2}$ orbital.

The available information on the excited states in ^{199}Tl is very scarce and limited to a few low-lying states which precludes one to get any idea about the $\nu i_{13/2}$ alignment. One of the first measurements of the excited states in ^{199}Tl was performed way back in 1970 by Newton *et al.* [20], with a few Ge(Li) detectors. Although only a few states could be identified in that work, but importantly, the deformed nature

---

*Corresponding author: sarmi@vecc.gov.in
†Present address: Prabhat Kumar College, Contai, Purba Medinipur, West Bengal, India.

of the $\pi h_{9/2}$ state was predicted by them. Information on the low-spin states in ^{199}Tl was also reported from the EC-decay study of ^{199}Pb [21]. In the last reported work on ^{199}Tl, a set of LaBr$_3$(Ce) detectors were used along with six HPGe detectors [22]. A few new states could be identified in that work, but the main focus of that experiment was to measure the lifetime of the excited states using the fast scintillator detectors in combination with the HPGe detectors.

In the present work, we have used the α induced fusion evaporation reaction to investigate the yrast and non-yrast states in ^{199}Tl as well as the band crossing behavior of the $\pi h_{9/2}$ band. With the availability of high efficiency, high resolution new generation HPGe clover detectors, it has become possible to obtain more complete information about the detailed band structures of ^{199}Tl.

II. EXPERIMENT

The excited states of ^{199}Tl were populated using a ^{197}Au$(\alpha, 2n)$ reaction with a 30 MeV α beam from the K-130 Cyclotron at VECC, Kolkata. The beam energy was chosen to maximize the population of the $2n$ evaporation channel. In the α induced fusion evaporation reaction, a unique reaction channel can be populated with a large cross section having very little overlap with the other neighboring neutron evaporation channels at a suitably chosen beam energy. The decaying γ rays from the excited states were detected using VECC Array for NUclear Spectroscopy (VENUS) [23] at VECC, consisting of six Compton-suppressed clover HPGe detectors. Two detectors were placed at forward 45° and 55°, two at 90°, and the remaining two at the backward 30° angles with respect to the beam direction and at a distance of ~26 cm from the target position. The signals from the clover detectors were processed using 16 channel Mesytec amplifiers and the standard NIM analog electronics were used for the BGO shields and for other trigger logics. The data were collected with 13 bit high resolution 32 channel VME ADCs and VME based data acquisition system using LAMPS [24]. Data were taken with two master trigger conditions, singles mode (at least one clover "fires") for the angular distribution measurement and doubles mode (at least any two clovers "fire") for the γ-γ coincidence measurements. Six Time-to-Amplitude Converters (TACs) were used to measure the time between the individual OR of all the crystals of a clover detector and the master trigger. Another TAC was used for timing measurements of the events with respect to the RF signal from the cyclotron. The efficiency and energy calibrations of each detector were carried out using ^{133}Ba and ^{152}Eu standard radioactive sources, placed at the target position.

Data were sorted using LAMPS [24], INGASORT [25], and RADWARE [26] software packages. A γ-γ matrix was generated to verify the coincidence relations of the γ rays. A matrix was also formed using the data from the two detectors in the backward (30°) angle in the y axis and the other two detectors at 90° angle in the x axis to find out the Directional Correlation from Oriented states (DCO ratio) [27] for various transitions. The 90° detectors are used for the measurements of Integrated Polarization from Directional Correlation of Oriented states (IPDCO) [28,29] for assigning the parity of the states.
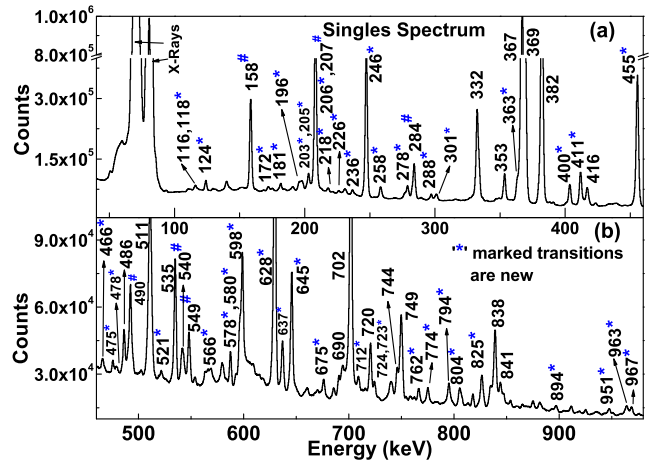

FIG. 1. Total spectrum of γ rays detected in singles trigger condition. (a) The lower energy part (up to 460 keV) and (b) the higher energy part (461–980 keV) of the spectrum. The new peaks observed in the present work are marked with '*'. The other transitions, marked with '#' are from decay of ^{199}Tl or from neighboring nuclei

III. DATA ANALYSIS

The raw data from all the 24 crystals were calibrated and gain matched to 0.3 keV/ch to form six addback spectra from individual Clovers. All these addback spectra were then used for generating the E_γ-E_γ two-dimensional (2D) matrix by selecting the prompt part of the TAC spectrum of each clover as well as the prompt part of the RF-γ TAC to select the prompt γ-γ coincidence events.

A spectrum obtained from the singles trigger mode is shown in Fig. 1. It is clearly seen from Fig. 1 that almost all the γ rays observed in this singles spectrum belong to ^{199}Tl. Other than the known transitions, the new transitions from the present measurement are marked with an asterisk '*'. All the other transitions, marked with '#' are either from the β decay of ^{199}Tl to ^{199}Hg or from neighboring nuclei which were also populated in the above reaction but with very less cross sections. This indicates the advantage of using an α beam as in this case the choice of 30-MeV beam energy almost uniquely populated the ^{199}Tl nucleus with very small contamination from the other channels.

The angular distribution of the γ rays, the DCO ratios and the IPDCO values were used to determine the multipolarities and the natures (E/M) of the transitions in order to assign the spins and parities (J^π) of the states.

The intensity distribution of the transitions from the singles data, after correcting for the efficiency of the respective detectors, is used for fitting the experimental angular distribution by the well-known Legendre polynomial function,

$$W(\theta) = a_0(1 + a_2 P_2(\cos\theta) + a_4 P_4(\cos\theta)), \qquad (1)$$

where θ is the detector angle with respect to the beam axis and a_0 is the normalization parameter. The value of these angular distribution coefficients (a_0, a_2, a_4) could be utilized to confirm the multipolarity as well as the stretched and non-stretched natures of the transitions. Figure 2 represents the angular distribution of stretched dipole and stretched quadrupole
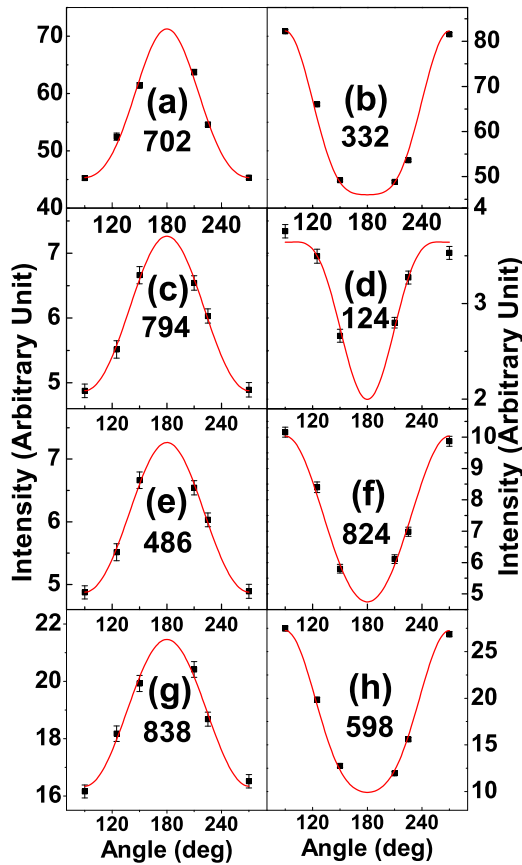
FIG. 2. Angular distribution of various transitions in ^{199}Tl obtained in the present work. (a),(c),(e),(g) are for quadrupole transitions. (b),(d),(f),(h) are for dipole transitions. The transition energies are also shown in each plot.

transitions from the current data. The 702 keV and 332 keV transitions are well known from the previous work [22] as pure quadrupole and dipole, respectively, and can be clearly verified from the nature of their fit. Multipolarity of the two newly assigned transitions of energy 794 keV (quadrupole) and 124 keV (dipole) can also be inferred. The 486 keV transition was previously assigned as $M1$ which seems to be of higher multipolarity (quadrupole) from the current angular distribution analysis. The dipole nature of the 598 keV transition could only be confirmed from its angular distribution, shown in Fig. 2(h), as the DCO ratio for this transition, in a gate of stretched transition, was not possible to obtain from the current data. The angular distributions from the singles data reliably represent the multipolarities of the new transitions as there are no other contamination in the spectra.

The multipolarity of most of the transitions, however, was obtained from the DCO ratios (R_{DCO}), defined by

$$R_{DCO} = \frac{I_{\gamma_1} \text{ at } \theta_1, \text{ gated by } \gamma_2 \text{ at } \theta_2}{I_{\gamma_1} \text{ at } \theta_2, \text{ gated by } \gamma_2 \text{ at } \theta_1}. \tag{2}$$

For the present measurement, the DCO matrix, as mentioned above, was used. The x and y axes of this asymmetric γ-γ matrix are the addback spectra of the two 90° detectors and of two backward 30°, respectively. The DCO ratio of a transition (γ_1) is then obtained from the ratio of its intensities at two

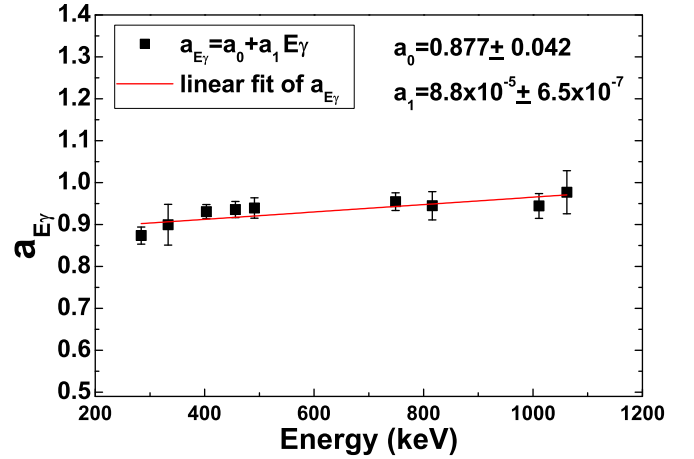FIG. 3. Asymmetry factor from various decay transitions in ^{199}Hg produced in the present work and linear fit of that with respect to energy.

angles θ_1 (30°) and θ_2 (90°) gated by another transition (γ_2) of known multipolarity, as per the expression (2). Typical value of R_{DCO} for a dipole or quadrupole transition (for γ_1) comes out to be 1.0 when gated by a transition of same multipolarity (γ_2). But when gated by known quadrupole (dipole) γ_2 then the DCO ratio value comes out to be close to 0.5(2.0) for dipole (quadrupole) transition. This definition is only true when both γ_1 and γ_2 are the stretched transitions, and the mixing ratio (δ) of the higher multipole order is small.

The parities of most of the excited states, populated in the present work could be assigned from the polarization measurements by exploiting the close packed configuration of four Ge crystals in a Clover detector. Compton scattering cross section of the emitted γ rays are used for the information regarding the type (electric or magnetic) of the transitions from the (IPDCO) asymmetry parameter following the prescription of Refs. [28,29]. The 90° detectors are used for this purpose to maximize the sensitivity of the polarization measurements. The IPDCO asymmetry parameter ((Δ_{IPDCO}) is defined as

$$\Delta_{IPDCO} = \frac{a(E_\gamma)N_\perp - N_\parallel}{a(E_\gamma)N_\perp + N_\parallel}, \tag{3}$$

where $N_\parallel$ and $N_\perp$ are the total photopeak counts of a γ ray, scattered in the planes parallel and perpendicular to the reaction plane, respectively. Here, $a(E_\gamma)[= \frac{N_\parallel}{N_\perp}]$ is the correction factor which addresses the geometrical asymmetry of the detector array or asymmetry in the response of the four crystals of a clover Ge detector and is obtained from the known γ rays from unpolarized source. In the present work, these are obtained from the decay γ rays of ^{199}Hg produced from the β decay of the ground state of ^{199}Tl having a half-life of 7.42 h [30]. The decay γ rays were recorded in the singles trigger mode in the same experiment at the end of the in-beam measurement. The values of $a(E_\gamma)$ for different γ-ray energies are shown in Fig. 3. The solid line in this plot is the fitting of the data points with a linear equation [$a(E_\gamma) = a_0 + a_1 E_\gamma$]. In order to obtain the Δ_{IPDCO} for a γ-ray transition, the corresponding value of the $a(E_\gamma)$ is taken from the above fit. In order to calculate Δ_{IPDCO}, two

TABLE I. The energies of the γ-ray transitions (E_γ), the energies of the initial levels (E_i), the spins and parities of the initial (J_i^π) and final (J_f^π) levels along with the relative intensities (I_γ), DCO ratios (R_{DCO}), and IPDCO values (Δ_{IPDCO}) for all the transitions in ^{199}Tl from the present work are shown. The proposed multipolarities of the γ rays are also mentioned.

E_γ (in keV)	E_i (in keV)	$J_i^\pi \rightarrow J_f^\pi$	I_γ(Err)[a]	R_{DCO}(Err)	Δ_{IPDCO}(Err)	Deduced multipolarity
(28.7)[b]	748.9	$9/2^- \rightarrow 5/2^+$	—	—	—	$M2$
111.2(2)	2944.0	$23/2^{(-)} \rightarrow 21/2^-$	0.92(16)	0.35(9)[c]	—	$(M1 + E2)$
116.0(1)	3060.0	$25/2^{(-)} \rightarrow 23/2^{(-)}$	0.42(12)	0.66(7)[d]	—	$(M1 + E2)$
116.1(1)	2195.3	$17/2^{(+)} \rightarrow 15/2^+$	0.34(13)	1.02(9)[e]	—	$(M1 + E2)$
118.3(1)	1985.2	$17/2^- \rightarrow 15/2^-$	0.31(13)	—	—	$(M1 + E2)$
123.8(1)	2203.0	$17/2^+ \rightarrow 15/2^+$	3.34(31)	1.05(3)[e]	—	$(M1)$
171.8(1)	2832.8	$21/2^- \rightarrow 19/2^-$	1.10(18)	0.41(7)[d]	—	$(M1 + E2)$
181.4(1)	2166.6	$19/2^- \rightarrow 17/2^-$	3.73(31)	0.61(2)[f]	$-0.17(12)$	$M1 + E2$
195.9(1)	2649.1	$21/2^{(+)} \rightarrow 19/2^{(+)}$	2.13(58)	0.44(4)[d]	$-0.06(5)$	$M1 + E2$
202.6(1)	2405.6	$19/2^+ \rightarrow 17/2^+$	7.09(43)	0.52(2)[d]	$-0.06(8)$	$M1$
204.8(2)	1410.2	$9/2^+ \rightarrow 7/2^+$	3.95(13)	—	—	$(M1 + E2)$
206.0(1)	1616.2	$9/2^+ \rightarrow 9/2^+$	0.40(3)	0.99(11)[g]	—	$M1 + E2$
217.8(1)	2866.9	$23/2^{(+)} \rightarrow 21/2^+$	1.71(22)	0.62(7)[d]	$-0.08(6)$	$M1 + E2$
226.0(1)	3286.0	$(27/2^-) \rightarrow 25/2^{(-)}$	0.45(11)	—	—	$(M1)$
236.3(2)	2641.9	$21/2^+ \rightarrow 19/2^+$	3.37(31)	0.45(4)[d]	$-0.09(4)$	$M1$
240.0(2)	2169.4	$(13/2^+) \rightarrow 11/2^+$	0.56(12)	—	—	—
257.9(2)	2453.2	$19/2^{(+)} \rightarrow 17/2^{(+)}$	5.93(38)	1.17(3)[e]	$-0.002(6)$	$(M1)$
269.6(1)	2254.8	$17/2^- \rightarrow 17/2^-$	0.40(13)	—	—	—
288.5(1)	1493.9	$9/2^+ \rightarrow 7/2^+$	3.08(21)	—	—	$M1$
300.8(1)	2706.4	$21/2^+ \rightarrow 19/2^+$	4.51(49)	0.48(3)[d]	$-0.03(2)$	$M1$
321.5(1)	2250.9	$13/2^+ \rightarrow 11/2^+$	1.14(15)	0.65(6)[h]	—	$(M1 + E2)$
326.4(1)	2405.6	$19/2^+ \rightarrow 15/2^+$	1.78(29)	1.04(16)[d]	0.17(14)	$E2$
328.0(1)	2194.9	$17/2^- \rightarrow 15/2^-$	2.31(29)	0.53(6)[d]	$-0.05(9)$	$M1$
332.2(1)	1450.5	$13/2^- \rightarrow 11/2^-$	47.21(7)	0.46(1)[d]	$-0.02(1)$	$M1$
338.9(1)	2809.7	$19/2^- \rightarrow 21/2^-$	0.27(4)	—	—	$(M1)$
353.3(1)	720.2	$5/2^+ \rightarrow 3/2^+$	52.6(9)	0.80(1)[i]	$-0.04(2)$	$M1 + E2$
363.2(1)	2079.2	$15/2^+ \rightarrow 13/2^-$	14.18(5)	—	—	$(E1)$[j]
366.9(1)	366.9	$3/2^+ \rightarrow 1/2^+$	76.22(17)	0.68(14)[k]	$-0.03(10)$	$(M1 + E2)$
369.4(1)	1118.3	$11/2^- \rightarrow 9/2^-$	100.0(2)	0.32(1)[f]	$-0.02(1)$	$M1 + E2$
382.0(1)	748.9	$9/2^- \rightarrow 3/2^+$	49.58(6)	—	—	$E3$[j]
387.9(4)	2254.8	$17/2^- \rightarrow 15/2^-$	1.08(65)	0.47(9)[d]	$-0.07(3)$	$M1$
400.0(1)	1810.2	$11/2^+ \rightarrow 9/2^+$	1.75(9)	1.06(7)[g]	$-0.16(4)$	$M1$
406.2(2)	2661.0	$19/2^- \rightarrow 17/2^-$	1.19(20)	0.26(11)[d]	$-0.05(4)$	$M1 + E2$
410.8(1)	1616.2	$9/2^+ \rightarrow 7/2^+$	0.33(5)	0.85(8)[i]	$-0.02(2)$	$M1 + E2$
416.4(1)	1866.9	$15/2^- \rightarrow 13/2^-$	18.97(67)	0.33(1)[c]	$-0.04(2)$	$M1 + E2$
417.1(1)	1911.0	$11/2^{(+)} \rightarrow 9/2^+$	1.83(12)	0.45(6)[k]	—	$(M1 + E2)$
418.5(1)	2889.3	$23/2^- \rightarrow 21/2^-$	2.16(16)	0.47(3)[f]	$-0.02(69)$	$M1$
423.2(1)	2626.2	$19/2^- \rightarrow 17/2^+$	3.14(29)	0.59(5)[d]	0.03(18)	$(E1)$
438.9(3)	2641.9	$21/2^+ \rightarrow 17/2^+$	1.19(10)	1.81(24)[e]	—	$(E2)$
466.1(1)	2661.0	$19/2^- \rightarrow 17/2^-$	2.09(29)	0.54(7)[c]	$-0.02(2)$	$M1$
475.0(1)	2191.0	$(15/2^-) \rightarrow 13/2^{(-)}$	1.31(1)	—	—	$(M1)$
477.5(1)	1682.9	$9/2^+ \rightarrow 7/2^+$	0.54(1)	0.55(3)[l]	—	$(M1 + E2)$
485.6(1)	2470.8	$21/2^- \rightarrow 17/2^-$	8.96(67)	1.05(2)[f]	0.15(8)	$E2$
500.6(1)	2430.0	$(-) \rightarrow 11/2^+$	0.68(7)	—	—	—
520.8(1)	2014.7	$13/2^- \rightarrow 9/2^+$	1.90(9)	0.94(12)[k]	$-0.03(3)$	$M2$
534.7(1)	1985.2	$17/2^- \rightarrow 13/2^-$	34.91(92)	1.09(2)[d]	0.08(5)	$E2$
566.0(1)	3272.4	$25/2^+ \rightarrow 21/2^+$	2.49(23)	2.01(69)[e]	0.05(3)	$E2$
578.0(1)	2832.8	$21/2^- \rightarrow 17/2^-$	1.08(31)	1.00(28)[d]	0.05(18)	$E2$
580.0(1)	2191.0	$(-) \rightarrow 13/2^-$	1.72(3)	—	—	—
597.7(1)	1716.0	$13/2^- \rightarrow 11/2^-$	33.40(49)	—	—	$(M1)$
628.7(1)	2079.2	$15/2^+ \rightarrow 13/2^-$	56.10(6)	0.55(1)[d]	0.02(5)	$E1$
637.9(1)	2832.8	$21/2^- \rightarrow 17/2^-$	0.83(27)	—	—	$(E2)$
643.1(1)	2809.7	$19/2^- \rightarrow 19/2^-$	1.30(27)	0.51(7)[f]	—	$(M1)$
645.2(1)	1394.1	$11/2^- \rightarrow 9/2^-$	12.40(5)	—	$-0.01(1)$	$M1$[j,m]

TABLE I. *(Continued.)*

E_γ (in keV)	E_i (in keV)	$J_i^\pi \rightarrow J_f^\pi$	I_γ(Err)[a]	R_{DCO}(Err)	Δ_{IPDCO}(Err)	Deduced multipolarity
674.9(1)	2168.8	$9/2^{(+)} \rightarrow 7/2^+$	1.51(7)	0.52(11)[k]	−	$(M1 + E2)$
690.0(1)	1410.2	$9/2^+ \rightarrow 5/2^+$	6.72(28)	1.03(5)[k]	0.01(4)	$E2$
701.6(1)	1450.5	$13/2^- \rightarrow 9/2^-$	45.44(6)	0.89(1)[f]	0.07(5)	$E2$
712.1(1)	3182.9	$25/2^+ \rightarrow 21/2^-$	0.56(7)	1.02(42)[f]	−0.21(7)	$M2$
720.2(1)	720.2	$5/2^+ \rightarrow 1/2^+$	15.24(9)	−	0.02(15)	$E2$[m]
722.7(1)	2889.3	$23/2^- \rightarrow 19/2^-$	0.79(9)	0.98(9)[f]	−	$(E2)$
724.0(1)	1929.4	$11/2^+ \rightarrow 7/2^+$	3.29(11)	1.06(3)[l]	0.15(10)	$E2$
736.0(1)	3206.8	$25/2^- \rightarrow 21/2^+$	3.29(11)	0.90(11)[f]	−0.02(2)	$M2$
744.4(1)	2194.9	$17/2^- \rightarrow 13/2^-$	10.15(52)	1.08(5)[d]	0.005(18)	$E2$
748.6(1)	1866.9	$15/2^- \rightarrow 11/2^-$	9.52(3)	1.14(4)[c]	0.04(6)	$E2$
761.7(1)	1481.9	$9/2^{(+)} \rightarrow 5/2^+$	3.52(21)	0.90(11)[k]	−	$(E2)$
773.7(1)	1493.9	$9/2^+ \rightarrow 5/2^+$	4.95(23)	1.03(5)[k]	0.10(3)	$E2$
794.1(1)	2661.0	$19/2^- \rightarrow 15/2^-$	3.68(34)	0.88(6)[d]	0.06(6)	$E2$
804.3(1)	2254.8	$17/2^- \rightarrow 13/2^-$	5.70(38)	0.96(5)[d]	0.09(6)	$E2$
824.5(1)	2809.7	$19/2^- \rightarrow 17/2^-$	0.83(20)	0.63(9)[d]	−0.02(1)	$M1 + E2$
838.5(1)	1205.4	$7/2^+ \rightarrow 3/2^+$	13.55(5)	1.06(3)[h]	0.03(3)	$E2$
840.7(1)	2250.9	$13/2^+ \rightarrow 9/2^+$	3.79(5)	1.18(19)[k]	0.10(9)	$E2$
896.3(1)	3367.1	$25/2^- \rightarrow 21/2^-$	1.10(20)	1.02(12)[f]	0.06(13)	$E2$
902.6(1)	2832.0	$(−) \rightarrow 11/2^+$	−	−	−	(-)
950.8(1)	2880.2	$(15/2^+) \rightarrow 11/2^+$	−	−	−	$(E2)$
962.7(1)	1682.9	$9/2^+ \rightarrow 5/2^+$	2.20(2)	1.04(7)[k]	0.02(9)	$E2$
967.1(1)	1716.0	$13/2^- \rightarrow 9/2^-$	0.97(2)	−	0.07(10)	$E2$

[a]Relative γ-ray intensities are estimated from prompt spectra and normalized to 100 for the total intensity of 369.4-keV γ ray.
[b]Unobserved transition, adopted from Ref. [22].
[c]From 794.1 keV ($E2$) DCO gate.
[d]From 701.6 keV ($E2$) DCO gate.
[e]From 628.7 keV ($E1$) DCO gate.
[f]From 534.7 keV ($E2$) DCO gate.
[g]From 353.3 keV ($M1 + E2$) DCO gate.
[h]From 724.0 keV ($E2$) DCO gate.
[i]From 366.9 keV ($M1 + E2$) DCO gate.
[j]Adopted from Ref. [20] or [22].
[k]From 720.2 keV ($E2$) DCO gate.
[l]From 838.5 keV ($E2$) DCO gate.
[m]Multipolarity has been found from angular distribution.

asymmetric E_γ-E_γ matrices were formed. One of which (parallel matrix) has total photopeak counts of parallel scattered events of the two 90° detectors in the x axis and total photopeak counts of all coincidence events from the other detectors in the y axis. Another (perpendicular) matrix has the same data in the y axis but the x axis contains perpendicular scattered events of the clover detectors at 90° angle. From the projected spectra of the above mentioned parallel and perpendicular matrices, the number of counts in the perpendicular ($N_\perp$) and parallel ($N_\parallel$) scattering for a given γ ray were obtained. The positive and negative values of Δ_{IPDCO} correspond to the electric and magnetic transitions, respectively, which, for various transitions in ^{199}Tl, are given in Table I. The DCO ratio and the Δ_{IPDCO} values of various known and new transitions are also shown in Fig. 4.

IV. RESULTS

The level scheme of ^{199}Tl, as obtained in the present work is shown in Fig. 5. The level scheme is significantly extended compared to the previous work [22] establishing a number of few bands with different configurations with the placement of 53 new transitions. These bands and sequences of transitions are named as B1, B2, B3, B4, B5, B6, B7 in Fig. 5 for the convenience of describing them. The level scheme has been based on the coincidence relationships, relative intensities among the transitions, and the spin-parity assignments of the associated energy levels from angular distributions, R_{DCO}, and Δ_{IPDCO} values. The energy of the γ-ray transitions measured in this work, the energy of the initial levels, the spins and parities of the initial and final levels along with the relative intensities, DCO ratios, and IPDCO values for all the transitions in ^{199}Tl observed in the present work are tabulated in Table I.

The level scheme has been extended in two parts, one corresponds to the bands B5, B6, and B7 which bypass the known 28.4 ms $9/2^-$ isomer [20]; and the second, above this isomer. The level 748.9 keV was known to be of $J^\pi = 9/2^-$ from the previous decay study of ^{199}Pb [21], and from Ref. [31] by pulse beam method and due to the large spin difference with the level below (366.9 keV of $3/2^+$ spin) it results as
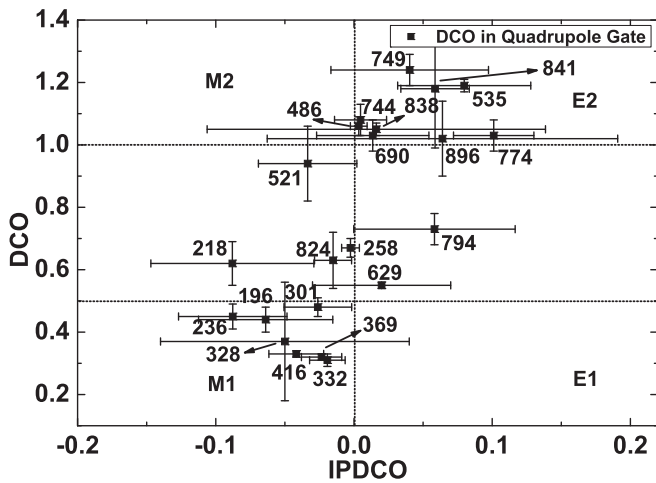
FIG. 4. DCO ratio vs polarization asymmetry (Δ_{IPDCO}) of various transitions in ^{199}Tl obtained from different quadrupole gates as indicated. The dotted lines parallel to the x axis correspond to the values for dipole and quadrupole transitions in a pure quadrupole gate, respectively, and are shown to guide the eye. The dotted line parallel to the y axis is to guide the eye for $+ve$ and $-ve$ values of Δ_{IPDCO} for electric and magnetic transitions, respectively.

an isomeric state with a half-life of 28.4 ms [20]. Band B1 in Fig. 5 is built on this isomer. The coincidence gate of the 332 keV transition in Fig. 6(a) shows all the transitions (except the 702 and 749 keV transitions which are parallel with respect to it) which belong to this band (B1) starting from the closest 416 keV transition to the topmost 226 keV transition. All the new transitions from the other sequences above the $9/2^-$ isomer, i.e., 328, 466, 388, 172, 794, 124, 218 keV, etc., are also seen in this spectrum. A spectrum gated by the newly identified transition at 794 keV is shown in Fig. 6(b) which shows only the transitions in coincidence with it, as placed in the level scheme, belonging to band B1. Transitions, which belong to band B1 but which are not in coincidence with 794-keV transitions are 328, 466, 638, 388, 406, 578, 744,

804 keV. They are placed parallel to the 794 keV transition in the level scheme. While comparing the coincidence gates of the 749 and 794 keV transitions from Figs. 6(b) and 6(c) it is clear that they are in coincidence with each other, while the cascade 416-332 keV (466-328 keV) corresponding to the crossover transition of 749 keV (794 keV) is only present in 794 keV (749 keV) gate confirming their relative placements in the level scheme. The DCO ratios of the 416, 388, 328, 406, 466, 172 keV transitions are found to be around 0.5 in gates on $E2$ transitions, which are marked as dipoles in Table I. Comparing the coincidence gates of 749 keV and 744 keV, two different cascades (466-328 keV and 406-388 keV) of $M1$ transitions appear between $19/2^-$ and $15/2^-$ spin levels. The 638, 466, and 172 keV γ rays are clearly present in the gate on 744 keV (not shown) whereas the absence of 328 keV and 794 keV γ rays confirms the 744 and 794 keV as parallel transitions. The crossover transitions corresponding to the uppermost levels of band B1 could not be identified from the present data. It is clearly seen from Figs. 6(b) and 6(c) that the 332 keV transition is present in the 794 keV gate whereas the 328 keV transition is present in the 749 keV gate which ensures the coincidence of the 328 keV transition with the 332 keV transition as well as the 749 keV transition. The spin and parity of the 2254.8 keV level has been fixed as $17/2^-$ from the $E2$ character of the 804 keV transition based on the IPDCO value of 0.09(6) and the DCO ratio value of 0.96(5) in a quadrupole gate (702 keV). The 578 keV transition also comes out to be of $E2$ nature and thus the J^π of 2832.8 keV level is fixed as $21/2^-$. The 172, 111, 116, and 226 keV transitions are present in all the gates shown in Fig. 6 but the 172-keV transition is not observed in the spectra gated by 578 or 638 keV transitions. This indicates the placement of the 172 keV γ ray is parallel with the 638 and 578 keV transitions, whereas the 111, 116, and 226 keV γ rays are placed on top of the band B1.

Though the Δ_{IPDCO} value of the 172 keV transition could not be determined, the J^π of the 2832.8 keV and 2661.0 keV levels, established it as a $M1$ transition. The J^π of the three
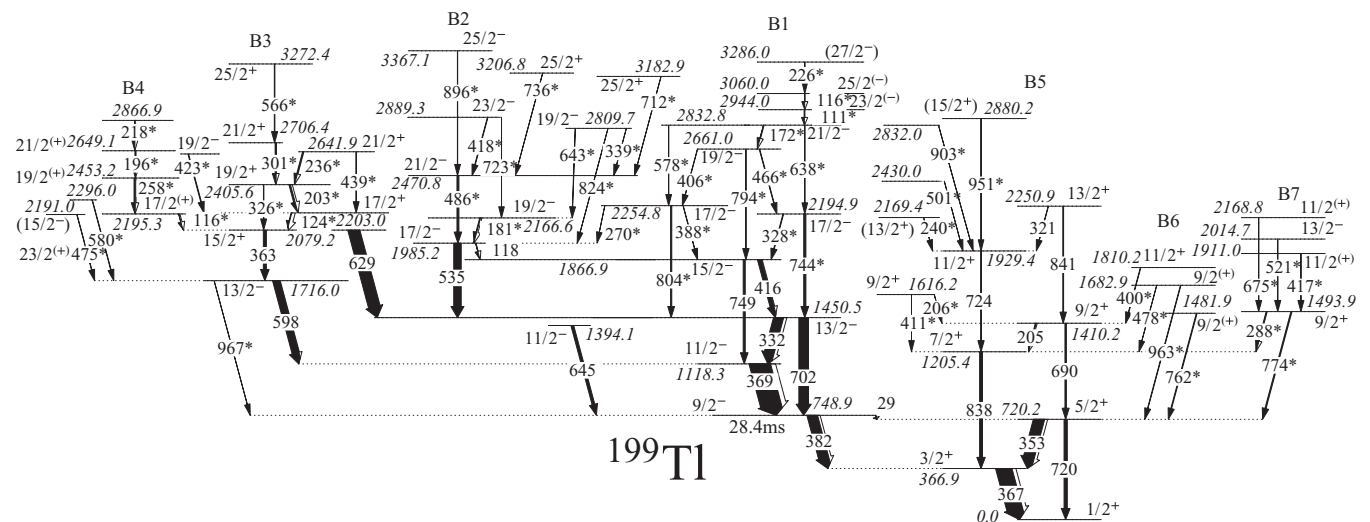

FIG. 5. Level scheme of ^{199}Tl, as obtained from the present work. New transitions are marked as '*'.
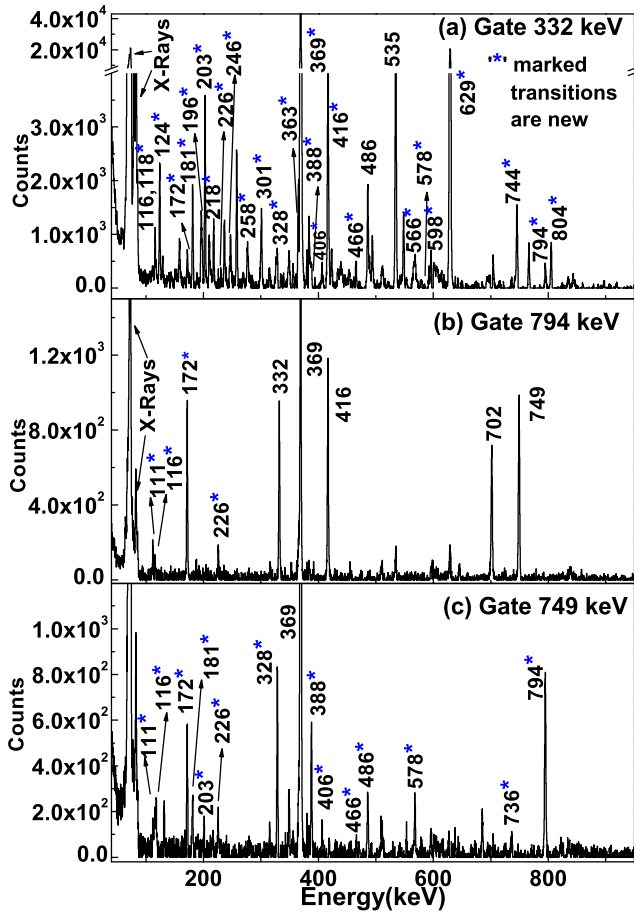
FIG. 6. Coincidence spectra corresponding to gates of (a) 332 keV, (b) 794 keV, (c) 749 keV transitions pertaining to band B1 and partly from bands B2, B3, B4 in ^{199}Tl. '∗' marked transitions are newly placed in the level scheme.

FIG. 7. Coincidence spectra gated by (a) 535 keV and (b) 486 keV corresponding to the transitions of band B2 in ^{199}Tl. '∗' marked transitions are newly placed in the level scheme.

top most levels in band B1 were determined only from the R_{DCO} values of the 111, 116 keV transitions, as their $\triangle_{IPDCO}$ could not be found. Thus the band B1 is extended up to J^{π} of $(27/2^{-})$ with the placements of these transitions.

A new band structure marked as band B2 in Fig. 5 has been established based on the level at 1985.2 keV which decays to the main band (B1) through the 535 keV and 118 keV transitions. The spin and parity of the 1985.2 keV level is fixed as $17/2^{-}$ on the basis of the $E2$ nature of the 535 keV transition, determined from its measured R_{DCO} value of 1.09(2) (in quadrupole gate) and $\triangle_{IPDCO}$ as 0.08(5).

The transitions 181, 270, 418, 486, 643, 712, 723, 824, and 896 keV, belonging to band B2, are observed in the coincidence spectrum gated by the 535 keV transition as shown in Fig. 7(a). But the 181, 270, 643, 824 keV lines are not observed in 486 keV gated spectrum of Fig. 7(b). The $\triangle_{IPDCO}$ value of the 723 keV transition could not be measured due to the contamination of 724 keV transition from band B5. But $M1$ character of the 418-keV transition, deduced from its DCO and $\triangle_{IPDCO}$ values, fixed the spin of the 2889.3 keV level as $23/2^{-}$. The 486 keV transition was identified as a $M1$ transition in the previous work [22]. However, in the present work, the R_{DCO} value of the 486 keV transition has been
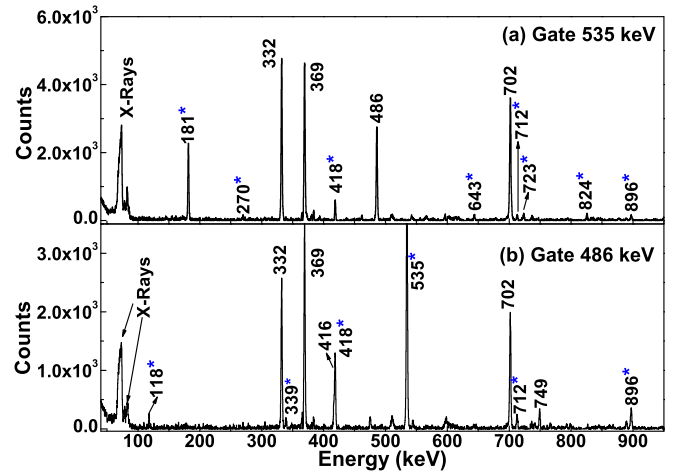
measured as 1.05(2) in the quadrupole gate of the 535 keV transition, and together with the positive value of the $\triangle_{IPDCO}$ it is suggested to be an $E2$ transition. Accordingly the J^{π} of the 2470.8 keV level has been assigned as $21/2^{-}$. Appearance of the 118 keV line and the absence of the 181 keV γ ray in the 486 keV gate also confirms that the 118 and 181 keV cascade (both $M1$) transitions and 535 and 486 keV cascade transitions are in parallel to each other. With the placement of these transitions and their crossovers in this band, the band B2 has been extended up to $25/2^{-}$. The presence of the connecting transitions between bands B1 and B2 are also seen in Fig. 7.

The $J^{\pi} = 15/2^{+}$ level at 2079.2 keV was known as the highest observed level in Ref. [20]. A cascade of transitions has been observed in the present work through the 124-keV transition, which is placed on top of this level as band B3. A separate branch, B4, has also been established above the 2079.2 keV level through the 116 keV γ ray. These two γ lines are clearly observed in the 629-keV gated spectrum shown in Fig. 8 (inset). The newly observed transitions in bands B3 and B4 are shown in the gated spectra of the 629-keV, 363-keV, and 124-keV transitions, showed in Figs. 8(a)–8(c), respectively. It can be seen that the 116-keV γ ray is not observed in the spectrum gated by the 124-keV transition, that establishes the two branches.

The 416 or 749 keV lines are absent in the gate on 629 keV while the 702 keV line is in coincidence with it. So the 629 keV γ ray connects with the main band (B1) through 1450.5 keV level. Both the 598 keV and 967 keV lines are present in the gate on 363 keV [Fig. 8(b)] whereas 629 keV and 702 keV are not present. These coincidence relations place the 363 keV in parallel with the 629 keV transition but in a cascade with the 967 keV or 598 keV transition. The absence (presence) of the 332 keV (369 keV) transition in the 363 keV gate established the connection of the 363 keV γ ray to band B1 only through the 598 keV line at 1118.3 keV. From DCO ratios, the multipolarities of the 124 keV and 116 keV transitions are assigned as $M1$. Therefore, positive parity is
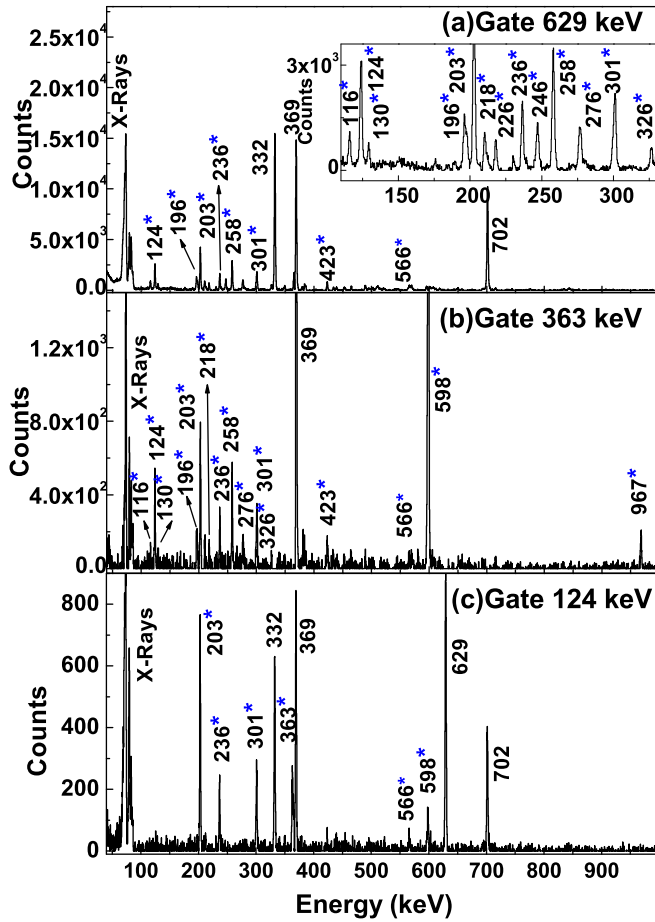
FIG. 8. Coincidence spectra corresponding to gates of (a) 629 keV, (b) 363 keV, (c) 124 keV transitions corresponding to bands B3 and B4 in ^{199}Tl. '*' marked transitions are newly placed in the level scheme.
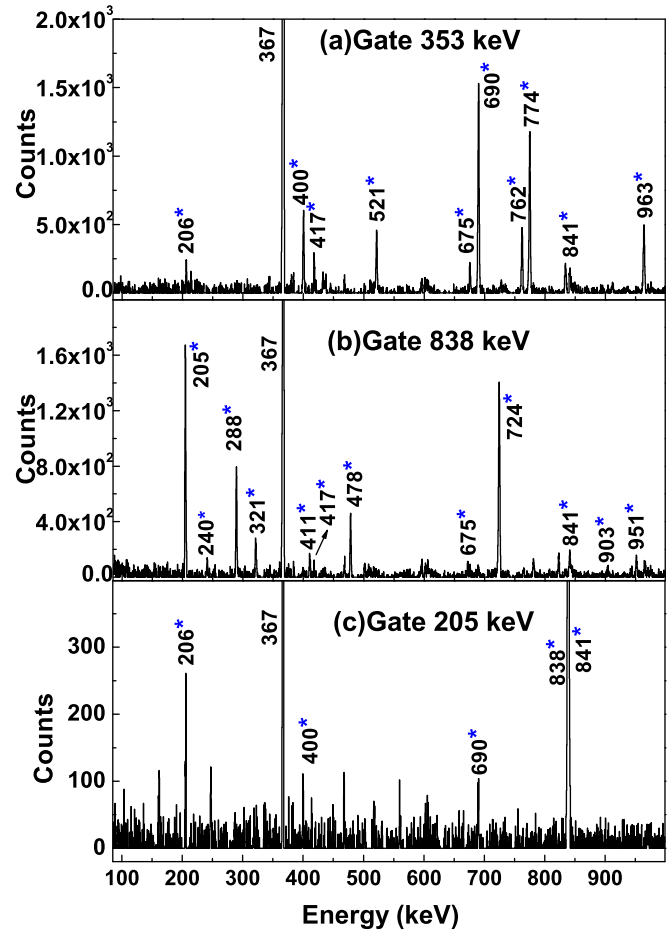

FIG. 9. Coincidence spectra corresponding to the gates of (a) 353 keV, (b) 838 keV, (c) 205 keV transitions corresponding to band B5 in ^{199}Tl. '*' marked transitions are newly placed in the level scheme.

assigned to bands B3 and B4. It is clearly seen from Fig. 8 that 326 keV does not appear in the spectrum gated by the 124 keV transition while it is present in both 629 keV [Fig. 8(a)inset] and 363 keV gates. Presence of a strong 203 keV line in coincidence with 363 keV transition establishes the 326 keV γ ray as a crossover $E2$ of the 124 and 203 keV cascade. The other transitions are placed in these two bands according to their coincidence relation and bands B3 and B4 are extended up to the excitation energy of 3272.4 keV and 2866.9 keV, respectively.

An independent level has been identified at 1394.1 keV excitation which is connected to the 748.9 keV level by a 645 keV transition. This level has been reported earlier in Ref. [20] but the spin-parity was not known properly. The R_{DCO} value of 645 keV transition could not be found due to the lack of suitable gating transition but the Δ_{IPDCO} value suggests it as magnetic transition. The angular distribution suggests this transition as a dipole one. Thus the J^{π} of the level is now assigned as $11/2^-$.

The positive parity levels below the long-lived $9/2^-$ isomer were mostly known from the previous work of Refs. [20,22]. The ground state of ^{199}Tl was assigned as $1/2^+$ from the

earlier study [20]. A band-like structure with sequences of $M1$ and crossover $E2$ transitions was reported in the earlier work [22]. This sequence of levels is shown as band B5 in level scheme (Fig. 5) obtained in the present work. Two cascades of $E2$ transitions are seen but some of the interconnecting $M1$ transitions are not observed. The 367 and 353 keV transitions are confirmed to be ($M1/E2$) transitions as stated from the earlier work. A 382 keV transition decays from the 748.9 keV to the 366.9 keV level. Δ_{IPDCO} value $-0.03(10)$ of the 367 keV transition has fixed the spin of the 366.9 keV level as $3/2^+$ and thus the 382 keV γ rays come out to be an $E3$ [20]. Figures 9(a)–9(c) shows the γ rays in coincidence with the 353 keV, 838 keV, and 205 keV transitions. From Fig. 9(a) it can be seen that almost all the transitions which belong to B5, B6, and B7 are present but not the 720, 838, 724, 411, 951, 903 keV γ rays, which are placed either parallel to or to a different branch in the level scheme. The DCO ratio and Δ_{IPDCO} of the 838 keV γ rays are 1.06(3) (in the quadrupole gate) and 0.03(3) which fixes the spin of the 1205.4 keV level as $7/2^+$ and the 838 keV γ ray as $E2$. The presence of the 724 keV and 951 keV in coincidence with the 838 keV γ ray and the absence of the 690, 720, and 353 keV transitions in the

coincidence spectrum gated on the 838 keV [Fig. 9(b)] prove the presence of two parallel cascades of $E2$ transitions. The Δ_{IPDCO} value 0.15(10) indicates the 724 keV line as an electric transition and in the 838 keV ($E2$) gate the $R_{\text{DCO}} = 1.06(3)$ value confirms it as an $E2$ transition. Therefore, the 724 keV ($E2$) gate was used to obtain the DCO ratio of some of the unknown transitions.

The nature of all the other transitions (240, 501, 903, 951 keV) beyond the 1929.4 keV level could not be obtained because of low statistics and thus all spins and parities of the levels above 1929.4 keV are tentatively assigned. In the 720 keV gate only the 690, 841, and 205 keV are present from the sequence B5. DCO ratios of 690 keV and 841 keV are 1.03(5) and 1.18(19), respectively, in the quadrupole gate on 720 keV which also assigns them as $E2$ and the J^{π} of the 2250.9 keV level is thus fixed at $13/2^+$. The presence of the 206 keV line and absence of the 411 keV transitions in the coincidence gate on 205 keV [Fig. 9(c)] assigns the 205–206 keV cascade across the 411 keV transition. According to the level scheme, the 690 keV transition should not come in coincidence with the 205 keV transition. On the other hand the 205 keV γ ray is in coincidence with the 838 and 841 keV transitions. But along with the 838, 841 keV transitions, the 690 keV line also appeared in the coincidence gate on 205 keV in Fig. 9(c) due to the contamination of the gate on 205 keV with the 206 keV transition. The DCO ratio value of the 206 keV transition has been found out to be 0.99(11) with respect to the 353 keV ($M1 + E2$) gate and thus its multipolarity is concluded as dipole. The Δ_{IPDCO} and R_{DCO} values of the 411 keV transition also suggest it as $M1 + E2$ nature and thus the J^{π} of the 1616.2 keV level is assigned as $9/2^+$, thereby fixing the nature of the 206 keV transition as a nonstretched $M1$ transition. The presence of the 321 keV line in both the 838 and 724 keV gates and the presence of the 205 keV line in both the 838 and 841 keV gates, establishes a series of decaying $M1$ transitions from $13/2^+$ to $11/2^+$ (321 keV), $9/2^+$ to $7/2^+$ (205 keV) and $5/2^+$ to $3/2^+$ (353 keV) levels between the two branches of $E2$ sequences in B5.

A set of new levels are found in B6 and B7 to be built by the two sequences of γ rays generated above the 720.2 keV level. All of these γ rays decay from sequences B6, B7, to B5 and are seen in Figs. 9(a)–9(c). The 1493.9 keV level (of sequence B7) decays to B5 by the 288 ($M1$) and 774 ($E2$) transitions. The nature of the 288 and 774 keV transitions are shown in Table I depending on the R_{DCO} and Δ_{IPDCO} values and thus the J^{π} of the 1493.9 keV level is established as $9/2^+$. Multipolarities of almost all the transitions belonging to B6 and B7 are found out from the quadrupole gate on 720 keV or the dipole gate on 353 keV, wherever possible. Few transitions are observed to be in coincidence with 774 and 288 keV and placed above the 1493.9-keV level. Multipolarity of 675 keV transition is concluded as dipole by its R_{DCO} value of 0.52(11) in 720 keV quadrupole gate. Similarly, with the DCO ratio and polarization asymmetry values, the 521 keV transition is found to be of $M2$ character and 417 keV is tentatively assigned as $M1$. The spin of 1682.9 keV level is fixed as 9/2 from the assigned multipolarity of the 963 keV transition obtained from its DCO ratio of 1.04(7) from the $E2$ gate

on 720 keV. Automatically the multipolarity of the 478 keV transition which decays from the 1682.9 keV to 1205.4 keV level is fixed as a dipole. The level at 1810.2 keV is assigned as $11/2^+$ from the $M1 + E2$ nature of the 400 keV transition determined from its Δ_{IPDCO} value of $-0.16(4)$ and the R_{DCO} value of 1.06(7) in the 353 keV ($M1 + E2$) gate. Another transition of 762 keV which can be seen in the 353 keV gate [Fig. 9(a)] is placed in B6 as an independent transition decaying from the 1481.9 keV level.

V. DISCUSSION

The level scheme of ^{199}Tl has been divided into a few band structures. The analog of band B1, on top of the $9/2^-$ isomer has been observed in all the odd-A Tl isotopes and has been interpreted as the one based on the intruder $\pi h_{9/2}$ configuration. In this work, this band has been extended and thus can be compared with the other neighboring odd-A Tl isotopes. At higher spins above $13/2^-$, this band has been observed to bifurcate into two structures. The states in band B2 with possibly three-quasiparticle (3qp) nature are yrast while the band B1 continues through the non-yrast states. Bands B3 and B4 are positive parity bands. The initial few states in the band-like structure B5 were already known, and the analogs are also known in the neighboring Tl isotopes, ^{195,197}Tl. These states correspond to the proton single particle states $s_{1/2}$ and $d_{3/2}$, lying below the $Z = 82$ shell closure. In the present work, these states have been extended through the observation of a sequence of positive parity non-yrast states in band B5 up to an excitation energy of 2.88 MeV. However, the spacing between the states in this band-like structure does not seem to correspond to a rotational band of a well deformed nucleus. A few more states have also been observed in the present work and are classified as B6 and B7 sequences in Fig. 5 which decay to the sequence B5.

The aligned angular momentum (i_x) vs rotational frequency ($\hbar\omega$) plot for the $\pi h_{9/2}$ bands of different odd-A Tl nuclei is shown in Fig. 10. The aligned angular momenta (i_x) of other observed band structures in ^{199}Tl are compared in Fig. 11 with the similar bands of the neighboring odd-A Tl isotope ^{201}Tl and of the even-even ^{198}Hg core. The band B1, with a $9/2^-$ band head, has a $h_{9/2}$ configuration as has been described in an earlier work [20] which continues up to about $9.5\hbar$ of spin. The i_x plot for this band shows a gain in alignment of more than $9\hbar$ corresponding to the alignment of a pair of neutrons in the $i_{13/2}$ orbital. Hence the upper part of this band corresponds to a configuration with 3qp, $\pi h_{9/2} \otimes \nu i_{13/2}^2$.

Band B2 is yrast beyond $7.5\hbar$, but as seen from Fig. 11 the gain in alignment for this band ($\sim 4\hbar$) is smaller than the 3qp part of band B1 (see Fig. 10). Therefore, the neutron alignments take place in the ($f_{5/2}$, $p_{3/2}$) orbital. Hence the configuration of band B2 is $\pi h_{9/2} \otimes \nu(j_-)^2$, where $j_- = f_{5/2}, p_{3/2}$.

The alignment plots for the other neighboring odd-A Tl isotopes are also shown in Figs. 10 and 11. It is interesting to note that the initial alignment pattern for band B1 in ^{199}Tl matches well with the other lighter Tl isotopes but the alignment for band B2 in ^{199}Tl is similar to that in ^{201}Tl. The gain in alignments are also very similar in these two cases.
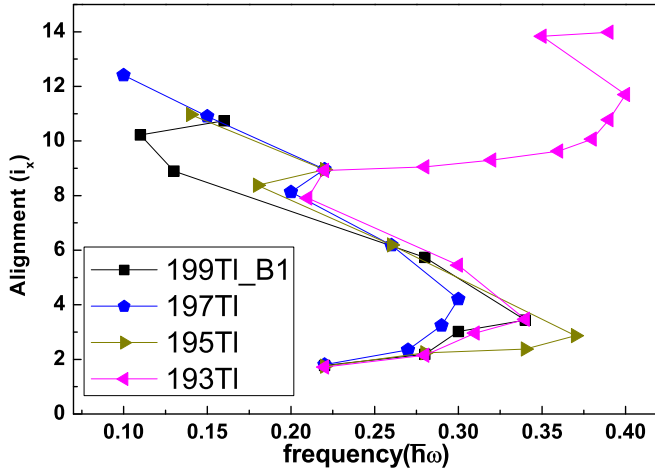
FIG. 10. Alignment plot for the $\pi h_{9/2}$ bands in odd-mass Tl isotopes. The level energies of the same bands of $^{193-197}$Tl are taken from Refs. [12–14], respectively. The Harris reference parameters are taken as $J_0 = 8\hbar^2 \text{MeV}^{-1}$ and $J_1 = 40\hbar^4 \text{MeV}^{-3}$.

The 3qp bands with configuration of $\pi h_{9/2} \otimes \nu(j_-)^2$ are yrast in case of ^{199,201}Tl whereas the 3-qp bands with configuration of $\pi h_{9/2} \otimes \nu i_{13/2}^2$ is yrast in case of lighter Tl isotopes. This change is, apparently, due to the change of neutron Fermi level and indicates that the neutron Fermi level lies close to the negative parity orbitals for $N \geqslant 118$.

The positive parity band in ^{199}Tl (marked as band B3 in the level scheme) also shows a rotational structure. However, the initial aligned angular momentum of about $6\hbar$ (Fig. 11) indicates the 3qp nature of this band. The alignment plot for the 5^- band in the neighboring even-even core of ^{198}Hg is shown in Fig. 11. The 5^- band in ^{198}Hg is originated from the $\nu(i_{13/2} \otimes j_-)$ configuration [32]. The similarity of

the initial alignments of these two suggests a similar neutron configuration for the band B3 in ^{199}Tl as for the 5^- band in ^{198}Hg. Hence a 3qp configuration of $\pi h_{9/2} \otimes \nu(i_{13/2} \otimes j_-)$ is assigned for this band. A strong transition from the band head of this band to the $h_{9/2}$ band supports this configuration. It may be noted, however, that the contribution of the $h_{9/2}$ proton to the observed i_x is very small indicating the involvement of the high-Ω component of the $h_{9/2}$ proton orbital, which is expected for an oblate deformation in ^{199}Tl. This band, however, could not be extended much for further discussion.

The level at the energy of 1394.1 keV can be identified as the state which is coming from the odd proton in ^{199}Tl occupying the $h_{11/2}$ orbital. All the odd-Tl isotopes from ^{195}Tl to ^{205}Tl have a similar level [33–37]. In the case of odd-A Au isotopes ($Z = 79$) from ^{191}Au to ^{197}Au [38–41] the $11/2^-$ state corresponding to this $\pi h_{11/2}$ configuration is a spin-gap isomer because this state can decay only by the transitions with large multipolarities as the available states below this level are mostly $1/2^+$, $3/2^+$, and $5/2^+$ (corresponding to the $s_{1/2}$, $d_{3/2}$, and $d_{5/2}$ configurations). However, as the proton Fermi level in Tl isotopes is higher in energy than in Au isotopes, the $11/2^-$ state lies at a relatively higher energy and the intruder $\pi h_{9/2}$ state lies at a lower energy (below the $11/2^-$ state) in Tl isotopes, creating a prompt decay path of the $11/2^-$ state to the $9/2^-$ state via low multipolarity transition as in the case of ^{199}Tl. Therefore, the presence of the intruder $\pi h_{9/2}$ orbital prevents the $11/2^-$ state in Tl isotopes from being an isomer.

To understand the characteristics of the band-like structure, marked as B5 in the level scheme of Fig. 5, its aligned angular momentum (i_x) is also plotted in Fig. 11 with the same Harris reference parameters ($J_0 = 8\hbar^2 \text{MeV}^{-1}$, $J_1 = 40\hbar^4 \text{MeV}^{-3}$) as the ones considered for bands B1, B2, and B3 of ^{199}Tl. It is clear from this plot that the same sets of Harris parameters does not hold for the structure B5 and a reduced J_0 and J_1 ($J_0 \sim 2.8\hbar^2 \text{MeV}^{-1}$, $J_1 \sim 27\hbar^4 \text{MeV}^{-3}$) would be required to fit the initial alignment of this sequence. This indicates that B5 has much less deformation compared to other bands in ^{199}Tl and the rotational model description may not hold well for the band-like structure B5.

The energy staggering, defined by $S(I) = [E(I) - E(I - 1)]/2I$, where $E(I)$ is the energy of the state with spin I, is plotted as a function of spin (I) for band B1 in Fig. 12, along with the same bands in $^{193-201}$Tl. It can be seen from this figure that the staggering plots of all odd-mass Tl isotopes show remarkable similarities, except for ^{201}Tl. The staggering in ^{201}Tl, however, matches quite well with that of band B2 in ^{199}Tl, suggesting a similar structure for these two bands. This supports our suggestion of the transitional nature of $N = 118$ in Tl isotopes in deciding the 3qp yrast configuration.

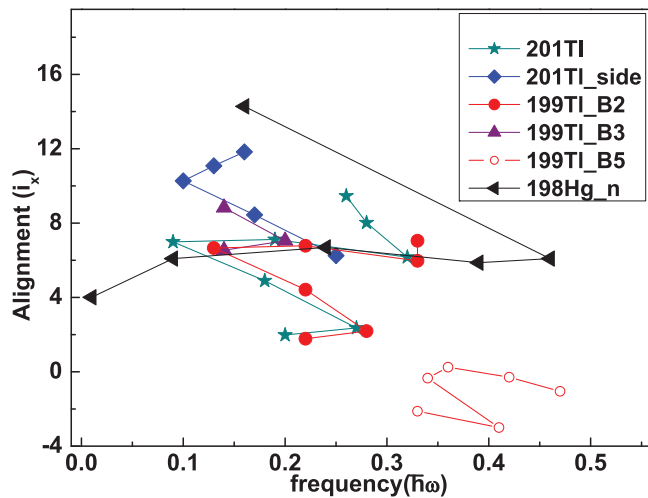FIG. 11. Alignment plot for the positive and negative parity bands of ^{199,201}Tl isotopes and comparison with the alignment of negative parity band of ^{198}Hg core. The level energies of the bands of ^{201}Tl and ^{198}Hg are taken from Refs. [15,32]. The Harris reference parameters are taken as $J_0 = 8\hbar^2 \text{MeV}^{-1}$ and $J_1 = 40\hbar^4 \text{MeV}^{-3}$.

VI. TRS CALCULATIONS

In order to have structural information on the different bands in ^{199}Tl, the Total Routhian Surface (TRS) calculations were performed by the Strutinsky shell correction method using deformed Woods-Saxon potential [42,43]. The universal parameter set was used for these calculations [44]. The total Routhian energies were calculated in (β_2, γ, β_4) deformation
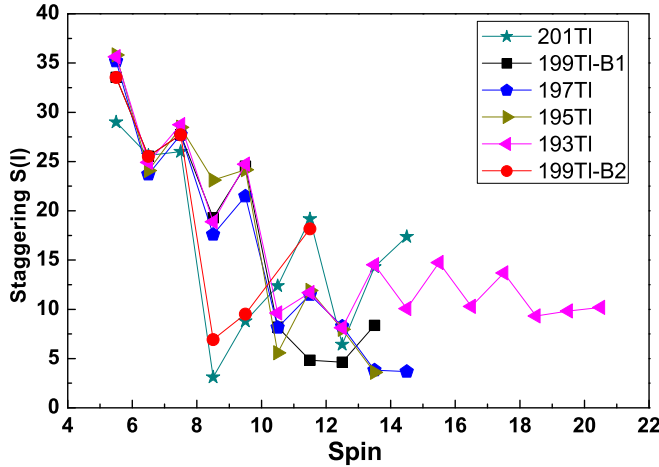
FIG. 12. Staggering $(S(I) = [E(I) - E(I-1)]/2I)$ plot for the $\pi h_{9/2}$ bands in odd-A Tl isotopes. Data for $^{193-201}$Tl are taken from Refs. [12–15,20], respectively.

mesh points with minimization on β_4. The procedure for such calculations has been outlined in Ref. [45]. The Routhian surfaces are plotted in the conventional β_2-γ plane. The calculations are performed for the one quasiparticle (1qp) negative parity configuration corresponding to the $\pi h_{9/2}$ band (B1), for the 1qp positive parity configuration corresponding to the $\pi s_{1/2}$ band, and for the 3qp positive parity configuration corresponding to the $\pi h_{9/2} \otimes \nu i_{13/2}(f_{5/2}p_{3/2})$ band.

The TRS plots for these three configurations close to the band heads are shown in Fig. 13. These plots are at the rotational frequency of $\hbar\omega = 0.11$ MeV. In these calculations the nuclear spin (I) is projected out and at near band-head frequencies, it corresponds to the single particle contribution. The surfaces corresponding to the 1qp negative parity configuration clearly show a minimum at an oblate deformation with $\beta_2 \sim 0.13$ and $\gamma \sim -60°$. The calculated projected spin for this configuration comes out to be $I = 4.5\hbar$, indicating an almost pure $\pi h_{9/2}$ configuration. A second minimum at a noncollective oblate deformation ($\gamma \sim +60°$) also appears for this configuration. For the case of the 1qp positive parity band for which $I = 0.5$ is calculated, the minimum appears close to the spherical shape [Fig. 13(b)], which is expected for the $\pi s_{1/2}$ configuration. This agrees with the observed band structure of band B5, which does not seem to be a well deformed one. Two minima, one at a collective oblate deformation with $\beta_2, \gamma \sim 0.14, -60°$ and $\sim 0.15, +40°$ are obtained for the 3qp configuration [Fig. 13(c)]. The difference between the two minima is less than 250 keV. At slightly higher frequencies the triaxial minimum becomes lower in energy. For this configuration, $I = 6.5$ is obtained for the band head which is close to the observed band B3 (in Fig. 5).

The variations of the calculated TRS energies, E_{TRS}, as a function of the triaxial deformation parameter γ for different rotational frequencies are shown in Fig. 14 for the 1qp negative parity and the 3qp positive parity configurations involving the $\pi h_{9/2}$ orbital. In these plots, the deformation parameter β_2 was kept around the values corresponding to the minimum in the two-dimensional TRS plots. It can be seen that the
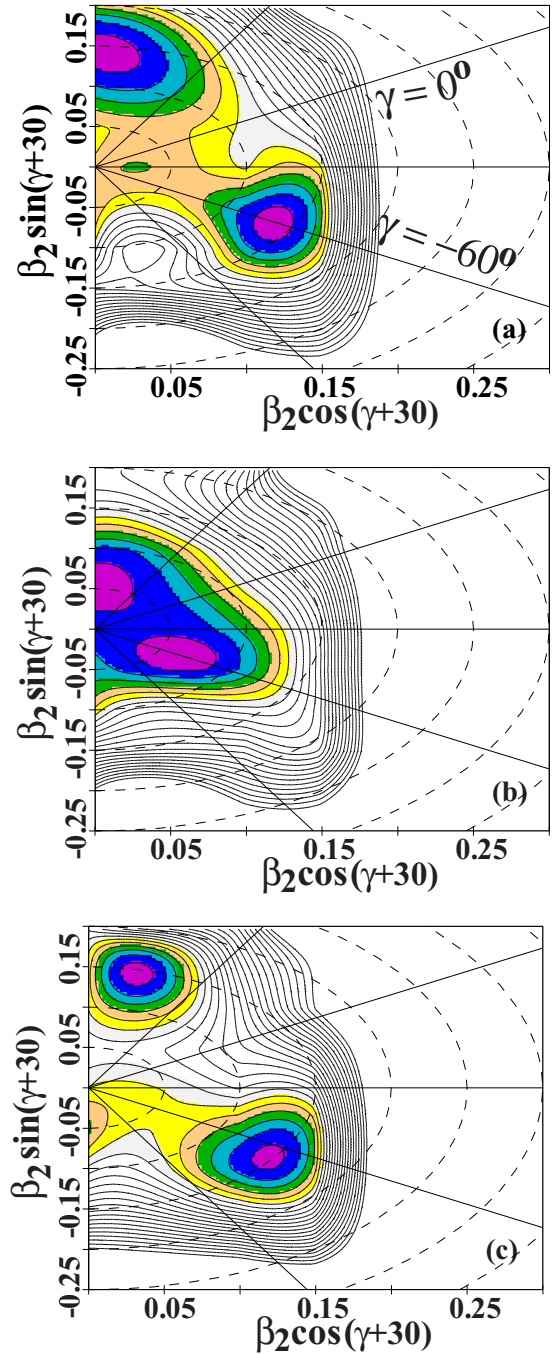

FIG. 13. Calculated TRS plots for the 1qp negative parity (a), 1qp positive parity (b), and 3qp positive parity (c) bands in ^{199}Tl. These are calculated at rotational frequency $\hbar\omega = 0.11$ MeV and the contours are 350 keV apart.

shape (corresponding to the minimum in the E_{TRS}) for the 1qp configuration [Fig. 14(a)] changes from axially deformed oblate ($\gamma \sim -60°$) at lower rotational frequencies to slightly triaxial with $\gamma \sim -75°$ at higher frequencies. On the other hand, for the 3qp positive parity band [Fig. 14(b)] two close lying minima are clearly seen at lower frequencies with some softness against γ near $\gamma \sim -60°$. At $\hbar\omega \sim 0.1$ MeV, E_{TRS} is minimum for a near-triaxial shape with $\gamma \sim +40°$. At a
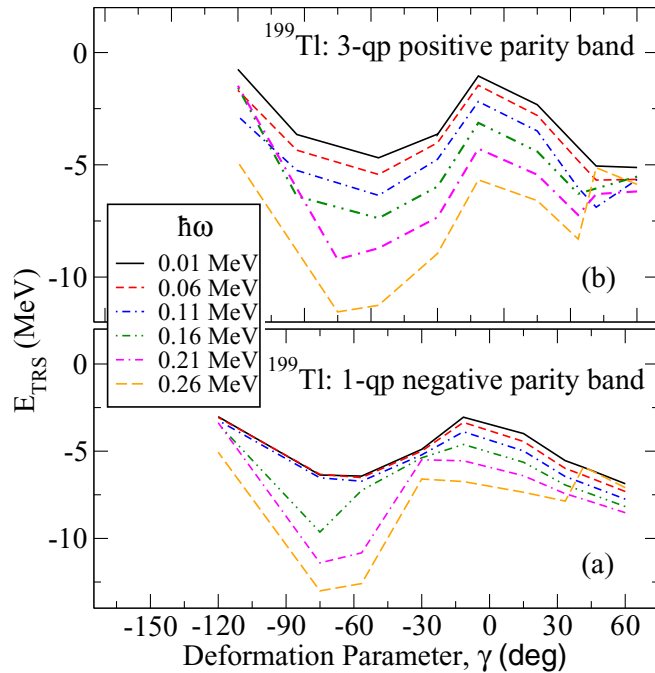
FIG. 14. The calculated TRS energy (E_{TRS}) as a function of the triaxial parameter γ for the (a) 1qp particle negative parity band and (b) 3qp positive parity band in ^{199}Tl for different rotational frequencies $\hbar\omega$.

six Compton suppressed clover HPGe detectors. The level scheme of ^{199}Tl has been extended considerably up to the excitation energy of $\sim$3.4 MeV and spin of $12.5\hbar$, with various structure of different configurations through the observation and placement of 53 new transitions in the level scheme. The spin and parity assignments were done by DCO, IPDCO, and angular distribution measurements. A new negative parity state with spin-parity $11/2^-$ has been identified and predicted to come from the involvement of the $\pi h_{11/2}$ orbital. It will be interesting to investigate the band structure on this state as seen in all nearby Au nuclei. A few band structures involving the intruder $\pi h_{9/2}$ have been observed in this odd-mass nucleus. The band structures are compared with those of the other odd-A Tl isotopes. It has been observed that the remarkable similarity of the low-lying states in the $\pi h_{9/2}$ band in odd-A Tl nuclei continues to persist in the $N = 118$ isotope. However, the yrastness of the 3qp configuration changes at $N = 118$ for ^{199}Tl which continues to ^{201}Tl.

The shape of ^{199}Tl for different configurations and its variation with rotational frequency are discussed in the light of the cranking model calculations with Woods-Saxon potential. Oblate deformation is obtained for the 1qp $\pi h_{9/2}$ band, whereas the low-lying 1qp positive parity band, corresponding to the $s_{1/2}$ configuration appears to be near spherical, in good agreement with the experimental observation. An interesting shape evolution from a coexisting and γ-soft shape to a triaxial shape at higher frequency, through an axially deformed oblate shape, is predicted in our calculations for the 3qp positive parity band. However, this cannot be confirmed from the present data obtained through α-induced reaction. Experiment with heavier beams and measurements of lifetimes to obtain $B(E2)$ values and deformation are warranted in future to understand the higher spin states and thereby the contribution of different high-j proton and neutron orbitals.

slightly higher frequency of $\hbar\omega \sim 0.16$ MeV, the minimum shifts to an axial oblate shape $\gamma \sim -57°$. At an even higher frequency, the minimum again shifts to around $\gamma \sim -75°$. The band structure, B3, corresponding to this configuration has been observed only up to a few states and these states seem to be due to the oblate deformation. It would be interesting to extend this band and measure the $B(E2)$ values up to higher frequencies to study the above prediction of shape change in this band.

VII. SUMMARY

Excited states of near yrast structure in ^{199}Tl have been populated by using the fusion evaporation reaction ^{197}Au(α, $2n$) at the beam energy of 30 MeV and studied by γ-ray spectroscopic techniques using the VENUS setup of

[1] H. Pai, G. Mukherjee, S. Bhattacharyya, M. R. Gohil, T. Bhattacharjee, C. Bhattacharya, R. Palit, S. Saha, J. Sethi, T. Trivedi, S. Thakur, B. S. Naidu, S. K. Jadav, R. Donthi, A. Goswami, and S. Chanda, Phys. Rev. C **85**, 064313 (2012).

[2] T. Roy *et al.*, Phys. Lett. B **782**, 768 (2018).

[3] P. L. Masiteng *et al.*, Phys. Lett. B **719**, 83 (1988).

[4] E. A. Lawrie, P. A. Vymers, J. J. Lawrie, C. Vieu, R. A. Bark, R. Lindsay, G. K. Mabala, S. M. Maliage, P. L. Masiteng, S. M. Mullins, S. H. T. Murray, I. Ragnarsson, T. M. Ramashidzha, C. Schuck, J. F. Sharpey-Schafer, and O. Shirinda, Phys. Rev. C **78**, 021305(R) (2008).

[5] A. Covello and G. Sartoris, Nucl. Phys. A **93**, 481 (1967).

[6] I. Hamamoto, Phys. Rep. **10**, 63 (1974).

[7] K. Heyde *et al.*, Phys. Rep. **102**, 291 (1983).

[8] M. Huyse *et al.*, Phys. Lett. B **201**, 293 (1988).

[9] S. Pilotte, C. H. Yu, H. Q. Jin, J. M. Lewis, L. L. Riedinger, Y. Liang, R. V. F. Janssens, M. P. Carpenter, T. L. Khoo, T. Lauritsen, F. Soramel, I. G. Bearden, C. Baktash, J. D. Garrett, N. R. Johnson, I. Y. Lee, and F. K. McGowan, Phys. Rev. C **49**, 718 (1994).

[10] P. B. Fernandez *et al.*, Nucl. Phys. A **517**, 386 (1990).

[11] F. Azaiez *et al.*, Z. Phys. A **338**, 471 (1991).

[12] W. Reviol *et al.*, Phys. Scr., T **56**, 167 (1995).

[13] J. O. Newton, F. S. Stephens, and R. M. Diamond, Nucl. Phys. A **236**, 225 (1974).

[14] R. M. Lieder *et al.*, Nucl. Phys. A **299**, 255 (1978).

[15] S. DasGupta, S. Bhattacharyya, H. Pai, G. Mukherjee, S. Bhattacharya, R. Palit, A. Shrivastava, A. Chatterjee, S. Chanda, V. Nanal, S. K. Pandit, S. Saha, J. Sethi, and S. Thakur, Phys. Rev. C **88**, 044328 (2013).

[16] J. Wrzesiński *et al.*, Eur. Phys. J. A **20**, 57 (2003).

[17] R. B. Firestone *et al.*, *Table of Isotopes* (John Wiley and Sons, New York, 1999).

[18] H. Pai, G. Mukherjee, S. Bhattacharya, C. Bhattacharya, S. Bhattacharyya, T. Bhattacharjee, S. Chanda, S. Rajbanshi, A. Goswami, M. R. Gohil, S. Kundu, T. K. Ghosh, K. Banerjee, T. K. Rana, R. Pandey, G. K. Prajapati, S. R. Banerjee, S. Mukhopadhyay, D. Pandit, S. Pal, J. K. Meena, P. Mukhopadhyay, and A. Choudhury, Phys. Rev. C **88**, 064302 (2013).

[19] S. Bhattacharya *et al.*, Phys. Rev. C **95**, 014301 (2017).

[20] J. O. Newton *et al.*, Nucl. Phys. A **148**, 593 (1970).

[21] R. E. Doebler and Wm. C. McHarris, Phys. Rev. C **2**, 2422 (1970).

[22] N. Marginean *et al.*, Eur. Phys. J. A **46**, 329 (2010).

[23] S. Bhattacharya *et al.*, DAE-BRNS Symp. Nucl. Phys. **61**, 98 (2016).

[24] http://www.tifr.res.in/~pell/lamps.html

[25] R. K. Bhowmik, S. Muralithar, and R. P. Singh, Proc. DAE Symp. Nucl. Phys. **44B**, 422 (2001).

[26] D. C. Radford, Nucl. Instrum. Methods Phys. Res. A **361**, 297 (1995).

[27] A. Kramer-Flecken *et al.*, Nucl. Instrum. Methods Phys. Res. A **275**, 333 (1989).

[28] K. Starosta *et al.*, Nucl. Instrum. Methods Phys. Res. A **423**, 16 (1999).

[29] Ch. Droste *et al.*, Nucl. Instrum. Methods Phys. Res. A **378**, 518 (1996).

[30] B. Singh, Nucl. Data Sheets **108**, 79 (2007).

[31] R. M. Diamond and F. S. Stephens, Nucl. Phys. A **45**, 632 (1963).

[32] C. Günther *et al.*, Phys. Rev. C **15**, 1298 (1977).

[33] K. H. Hicks, T. E. Ward, J. Wiggins, C. A. Fields, and F. W. N. deBoer, Phys. Rev. C **25**, 2710 (1982).

[34] L. L. Collins *et al.*, Diss. Abst. Int. **39B**, 3834 (1979).

[35] M. G. Slocombe, J. O. Newton, and G. D. Dracoulis, Nucl. Phys. A **275**, 168 (1977).

[36] D. Royer *et al.*, Nucl. Phys. A **158**, 516 (1970).

[37] J. A. Becker, R. G. Lanier, L. G. Mann, G. L. Struble, K. H. Maier, L. E. Ussery, W. Stoffl, T. W. Nail, R. K. Sheline, J. A. Cizewski, B. H. Erkkila, and J. Blomqvist, Phys. Rev. C **29**, 1268 (1984).

[38] H. Beuscher, P. Jahn, R. M. Lieder, and C. Mayer-Boricke, Z. Phys. **247**, 383 (1971).

[39] Z. Plajner, J. Frana, I. Rezanka, A. Spalek, and M. Fiser, Z. Phys. **233**, 122 (1971).

[40] K. Farzine and H. V. Buttlar, Z. Phys. **270**, 155 (1974).

[41] A. J. Haverfield, H. T. Easterday, and J. M. Hollander, Nucl. Phys. A **64**, 379 (1965).

[42] W. Nazarewicz *et al.*, Nucl. Phys. A **435**, 397 (1985).

[43] W. Nazarewicz *et al.*, Nucl. Phys. A **512**, 61 (1990).

[44] J. Dudek, Z. Szymanski, and T. Werner, Phys. Rev. C **23**, 920 (1981).

[45] G. Mukherjee *et al.*, Nucl. Phys. A **829**, 137 (2009).